PNAS MS# 2014-18674:
Daniel R. Lewis et al.,

Sugar-based Amphiphilic Nanoparticles Arrest Atherosclerosis In Vivo

SUPPLEMENTARY INFORMATION

Shell Material	D_h (nm)	PDI
M_{12}PEG	160	0.21
aM_{12}PEG	180	0.18
S_{12}PEG	240	0.18
bM_{12}PEG	175	0.21
cM_{12}PEG	190	0.17
T^{L}_{12}PEG	375	0.17
T^{D}_{12}PEG	320	0.17
T^{Meso}_{12}PEG	240	0.16
PS_{14}PEG	130	0.17

Fig. S1: Hydrodynamic diameter (D_h) and polydispersity index (PDI) of NP library.

NPs were fabricated from a library of amphiphile shells using a consistent hydrophobic core. NP size is partially determined by the LogP of the hydrophobic domain of the amphiphile, as stronger hydrophobic interactions lead to faster sequestration and smaller NPs. The low PDIs indicate monodisperse sizes with a narrow size distribution for a given NP formulation.

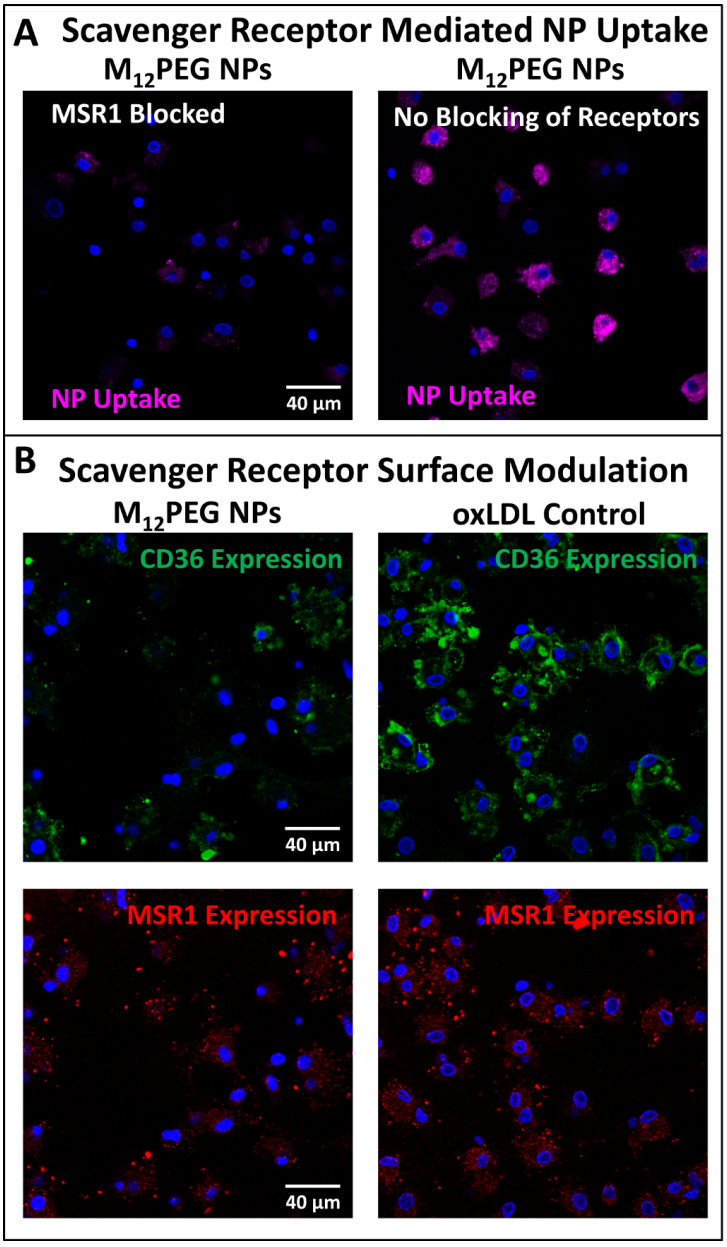

Fig. S2. NP interactions with and effects on scavenger receptors.

A) Receptor blocking studies revealed that M_{12}PEG NPs bind and are internalized via MSR1. B) M_{12}PEG is also able to modulate surface expression of the key scavenger receptors MSR1 and CD36. For this, hMDMs were either (A) incubated with polyinosinic acid (MSR1 inhibitor) for 2 hours and then incubated with 10^{-5} M NPs for 6 h or (B) co-incubated with 5 µg/mL oxLDL and 10^{-5}M NPs for 24 h and then evaluated by microscopy. Controls for (A) were non-blocked, basal hMDMs and controls for (B) were hMDMs treated with oxLDL only.

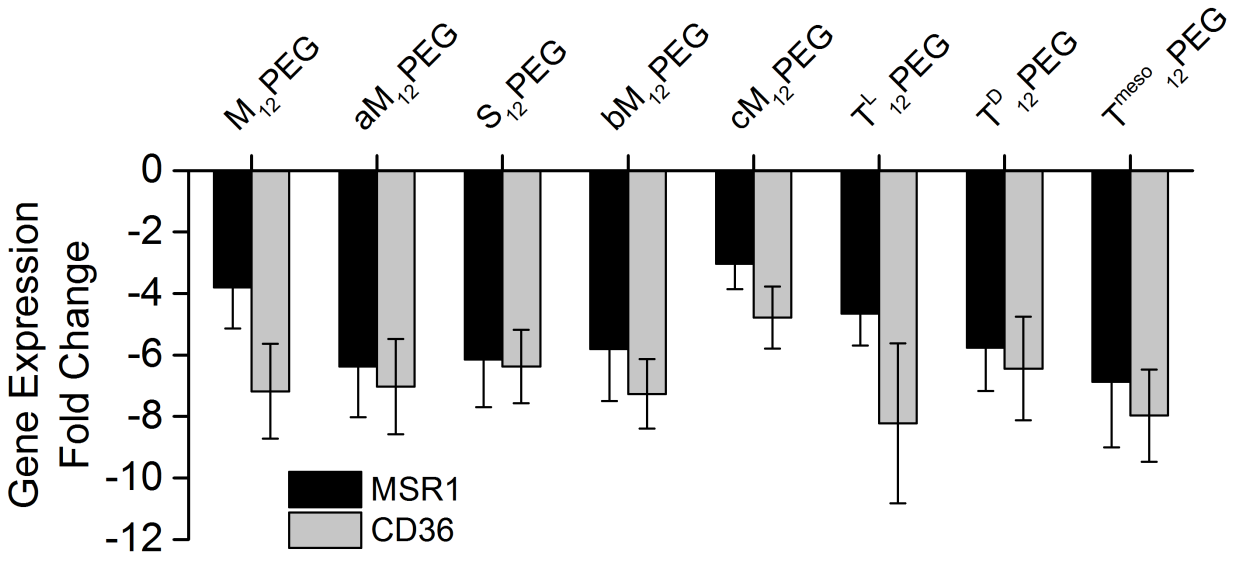

Fig. S3: Scavenger receptor gene expression in macrophages after treatment with NPs.

All NPs lowered expression of the scavenger receptors CD36 and MSR1, indicating reversal of the atherogenic phenotype. SR expression by macrophages is correlated to increased oxLDL uptake and plaque development *in vivo* (1). For this, hMDMs were treated with NPs for 24 h and assayed for changes in gene expression by qRT-PCR.

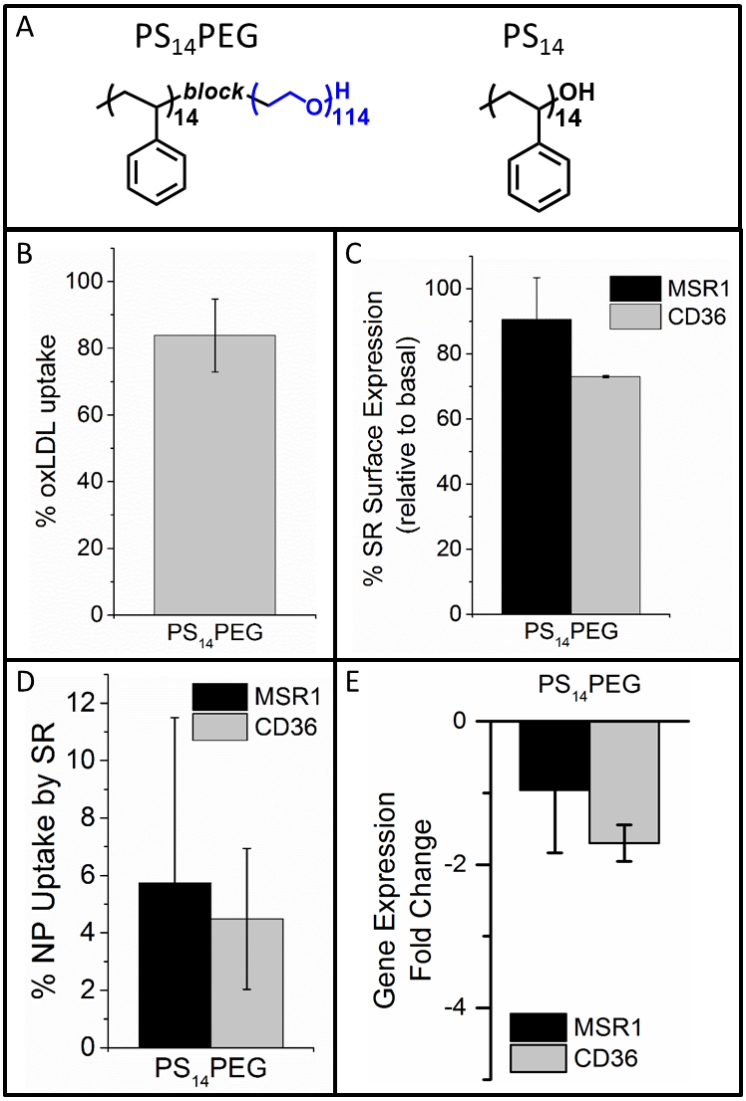

Fig. S4: Bioactivity screening for control NPs.

A) Control NPs were fabricated from polystyrene-*block*-poly(ethylene glycol) shells and polystyrene cores ($PS_{14}PEG$). $PS_{14}PEG$ NPs were tested for ability to block oxLDL uptake (B), SR surface expression changes (C), NP uptake by SR (D) and gene expression (E) in macrophages. $PS_{14}PEG$ NPs were not able to block oxLDL uptake and had minimal cellular uptake by scavenger receptors. $PS_{14}PEG$ also did not induce statistically significant changes in SR gene and protein expression, indicating a lack of *in vitro* bioactivity.

In vitro endpoint		Molecular descriptors that determine bioactivity
oxLDL uptake		**Mor17m:** signal 17 / weighted by mass 3D-MoRSE descriptors
		Mor32m: signal 32 / weighted by mass 3D-MoRSE descriptors
MSR1	NP binding	**Mor04m:** signal 4 / weighted by mass 3D-MoRSE
		Mor32m: signal 32 / weighted by mass 3D-MoRSE
	Gene expression	**J:** Balaban distance connectivity index – topological
		Mor18m: signal 18 / weighted by mass 3D-MoRSE
	Cell surface expression	**Mor17e:** signal 17 / weighted by atomic electronegativities 3D-MoRSE
		Mor19e: signal 19 / weighted by atomic electronegativities 3D-MoRSE
CD36	NP binding	**Mor26m:** signal 26 / weighted by mass 3D-MoRSE
		Mor27m: signal 27 / weighted by mass 3D-MoRSE
	Gene expression	**Ui:** unsaturation index - Molecular properties
		G2u: 2nd component symmetry directional WHIM index / unweighted
	Cell surface expression	**RDF120m:** Radial Distribution Function - 120 / weighted by mass
		RDF145m: Radial Distribution Function - 145 / weighted by mass

Fig. S5: Quantitative Structure Activity Relationship (QSAR) model for AM NP efficacy endpoints.

A parallel computation framework was established to link the biological antiatherogenic endpoints of the AM NPs to the molecular and structural features of the AM composition of the NP shells. This framework helps to unify the behaviors of the library of AMs within a self-consistent model and can be used as a basis to screen and predictively design improved AMs in the future.

In vitro endpoint efficacy values were used in conjunction with 3D structures of AMs to generate quantitative structure activity relationship (QSAR) models. Detailed 3D structures were computed previously by molecular dynamics simulation (2). Briefly, detailed 3D structures of AMs were computed previously by a two-step molecular dynamics simulation using a coarse-grained model for 400 ns followed by a detailed all-atom simulation for 10 ns.

Next, molecular descriptors were extracted from the 3D structures and correlated with variations in biological activity to determine the critical structural features. Molecular descriptors were calculated from the 3D structures using Dragon v.5.4 (Talete) and Molecular Operating Environment (MOE) v. 2013.08 (Chemical Computing Group). Partial least squares (PLS) analysis was performed for variations in biological activity (oxLDL uptake, CD36 and MSR1 gene expression, CD36 and MSR1 cell surface receptor expression, and NP uptake by CD36 and MSR1) in MOE. The descriptors represent complex chemical representations and encode a wide range of physiochemical properties (3). These descriptors predict biological efficacy of structures in a linear fashion ($r^2 > 0.9$ for predicted vs. experimental data).

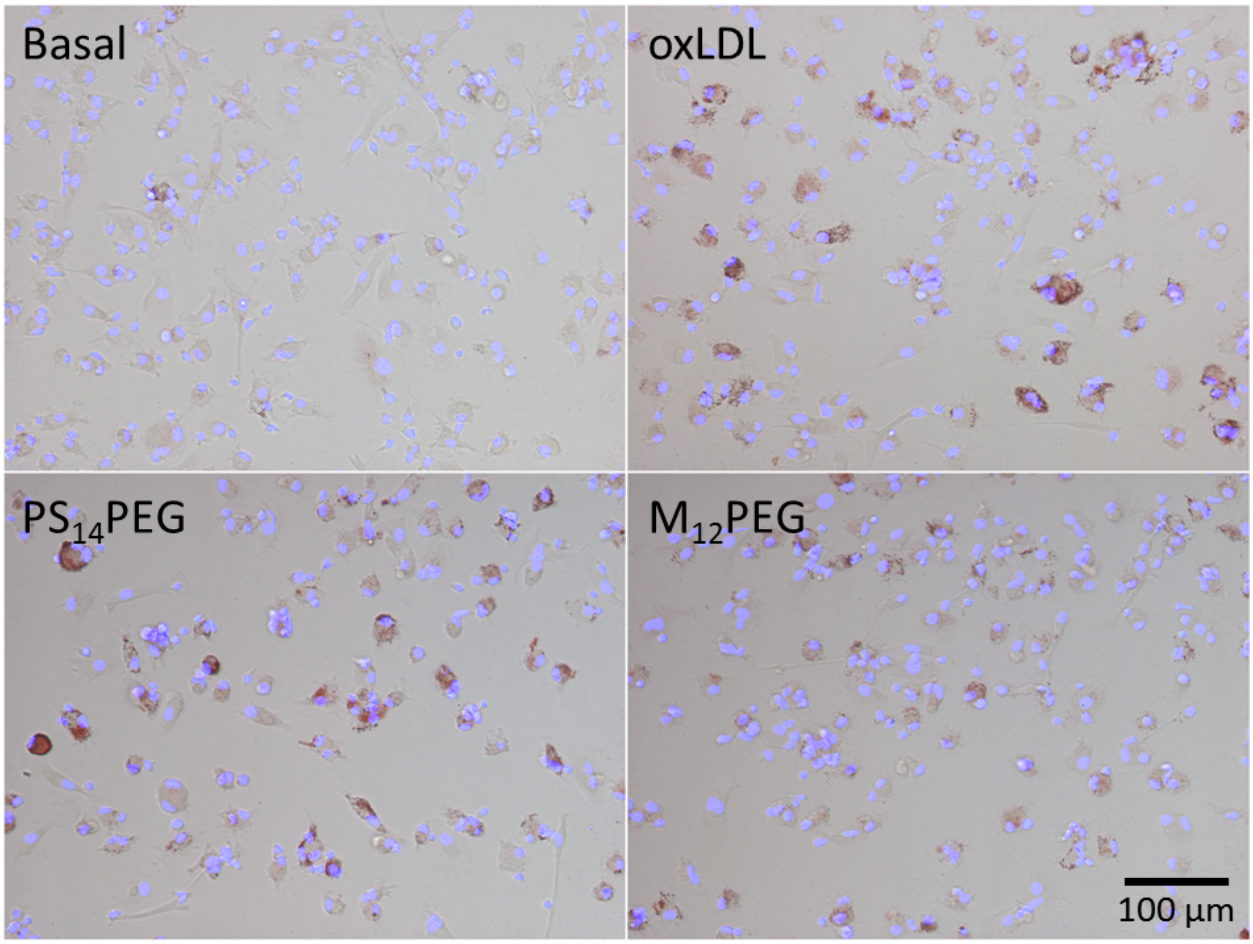

Fig. S6: Macrophage foam cell formation *in vitro*.

Foam cell formation resulting from unregulated lipid uptake by macrophages is a critical step in the atherogenic cascade and leads to vascular lipid burder. Consistent with oxLDL uptake studies, M_{12}PEG NPs significantly reduced oxLDL induced lipid accumulation and appear similar to basal cells. Control PS_{14}PEG NPs did not reduce lipid buildup and appear similar to the oxLDL only treatment condition. For this, hMDMs were incubated with 50 µg/mL unlabeled oxLDL, with or without NPs (10^{-5} M) for 24 hours in base media. Cells were then fixed in 4% PFA, washed with 60% isopropanol, stained with 3mg/mL Oil Red O in 60% isopropanol and counterstained with Hoechst 33342. Stained cells were imaged on a Nikon Eclipse TE2000S and representative images of were prepared with ImageJ.

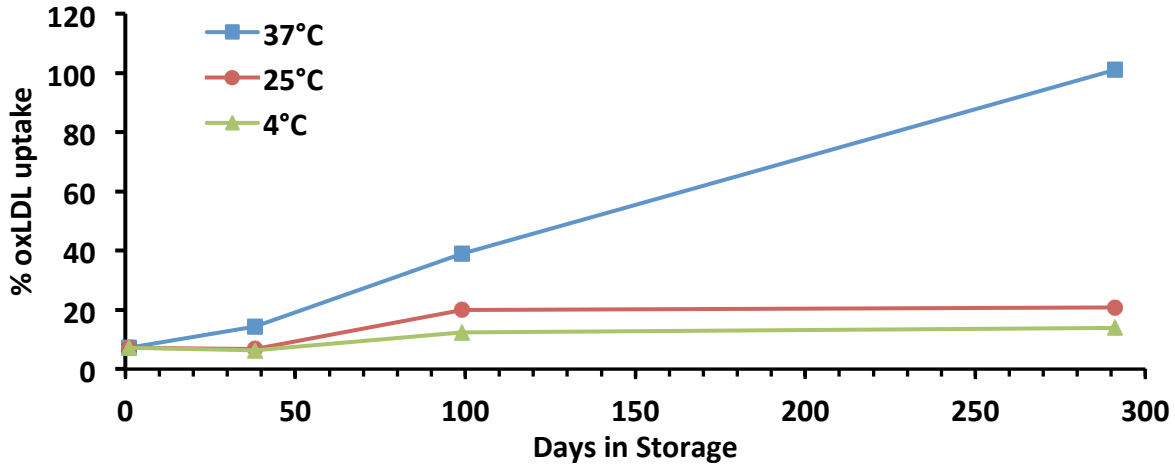

Fig. S7. Storage stability of M_{12}PEG AM NPs.

To demonstrate storage stability of the NPs, M_{12}PEG AM NPs were repeatedly assayed for bioactivity by examining their ability to inhibit oxLDL uptake in macrophages. When stored at 4°C and 25°C, efficacy did not decrease over the experimental period indicating highly stable NPs. Efficacy decreased over time when stored at 37°C. For this, NPs were stored at $5*10^{-4}$ M in PBS at 4°C, 25°C and 37°C, protected from light. To test activity, hMDMs were incubated with NPs and fluorescently labeled oxLDL for 24 h in media with serum before quantification of oxLDL uptake by flow cytometry.

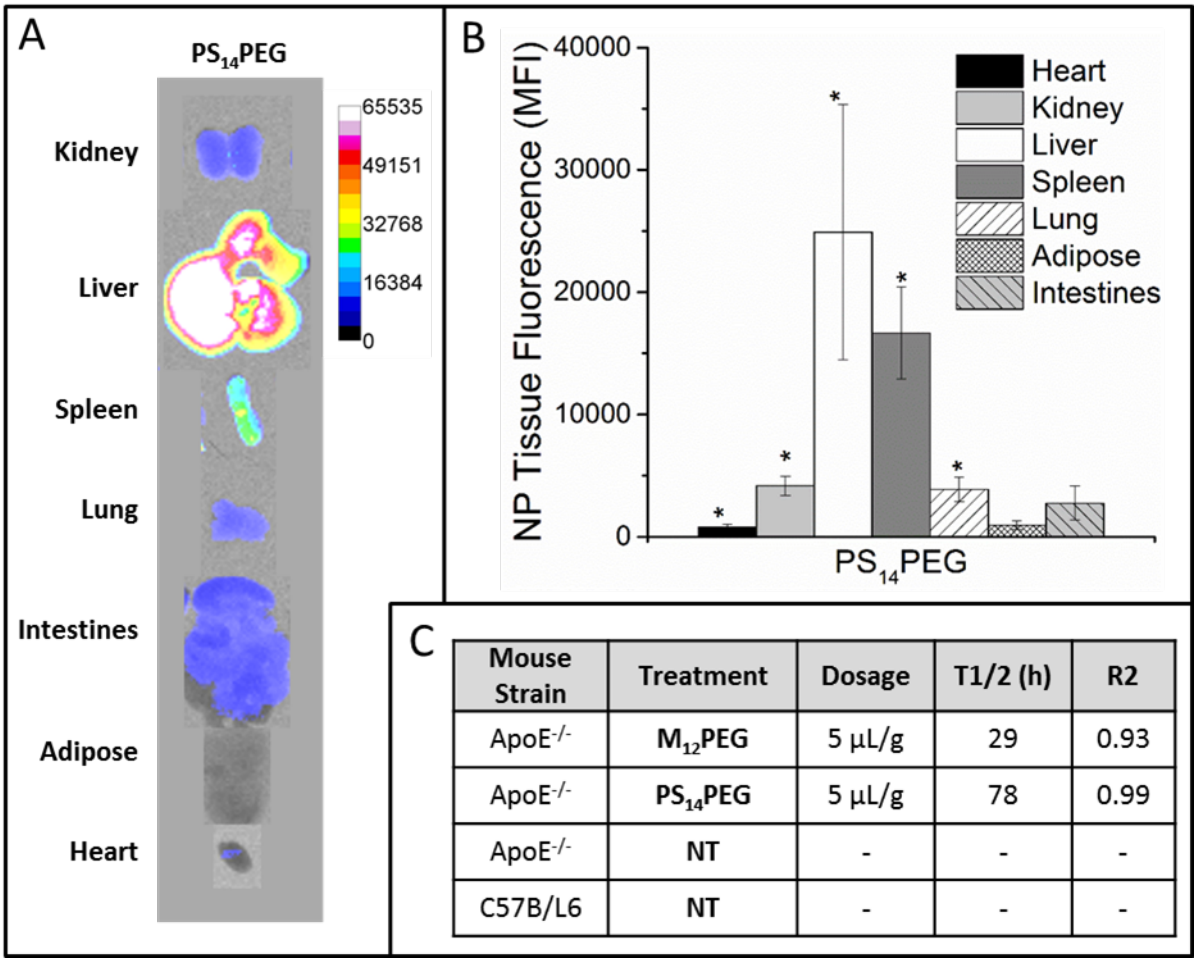

Mouse Strain	Treatment	Dosage	T1/2 (h)	R2
ApoE$^{-/-}$	**M_{12}PEG**	5 µL/g	29	0.93
ApoE$^{-/-}$	**PS_{14}PEG**	5 µL/g	78	0.99
ApoE$^{-/-}$	**NT**	-	-	-
C57B/L6	**NT**	-	-	-

Fig. S8: Biodistribution and pharmacokinetics for control NPs.

Control PS_{14}PEG NPs were administered in parallel to M_{12}PEG to ApoE$^{-/-}$ mice. A) *Ex vivo* organ fluorescence images and B) quantification of the mean fluorescence intensity (MFI) of the images revealed significant PS_{14}PEG accumulation in the liver and spleen as well as an increased presence in the lung, intestines, and kidneys. The significant off-target accumulation of PS_{14}PEG contrasts with the favorable biodistribution profile of M_{12}PEG. C) NP treatment groups and dosage administered to the specified mouse strain and *in vivo* NP half-lives were calculated using a one-compartment model. Asterisk (*) indicates $p < .05$ from control ApoE$^{-/-}$ mice that did not receive a treatment (NT).

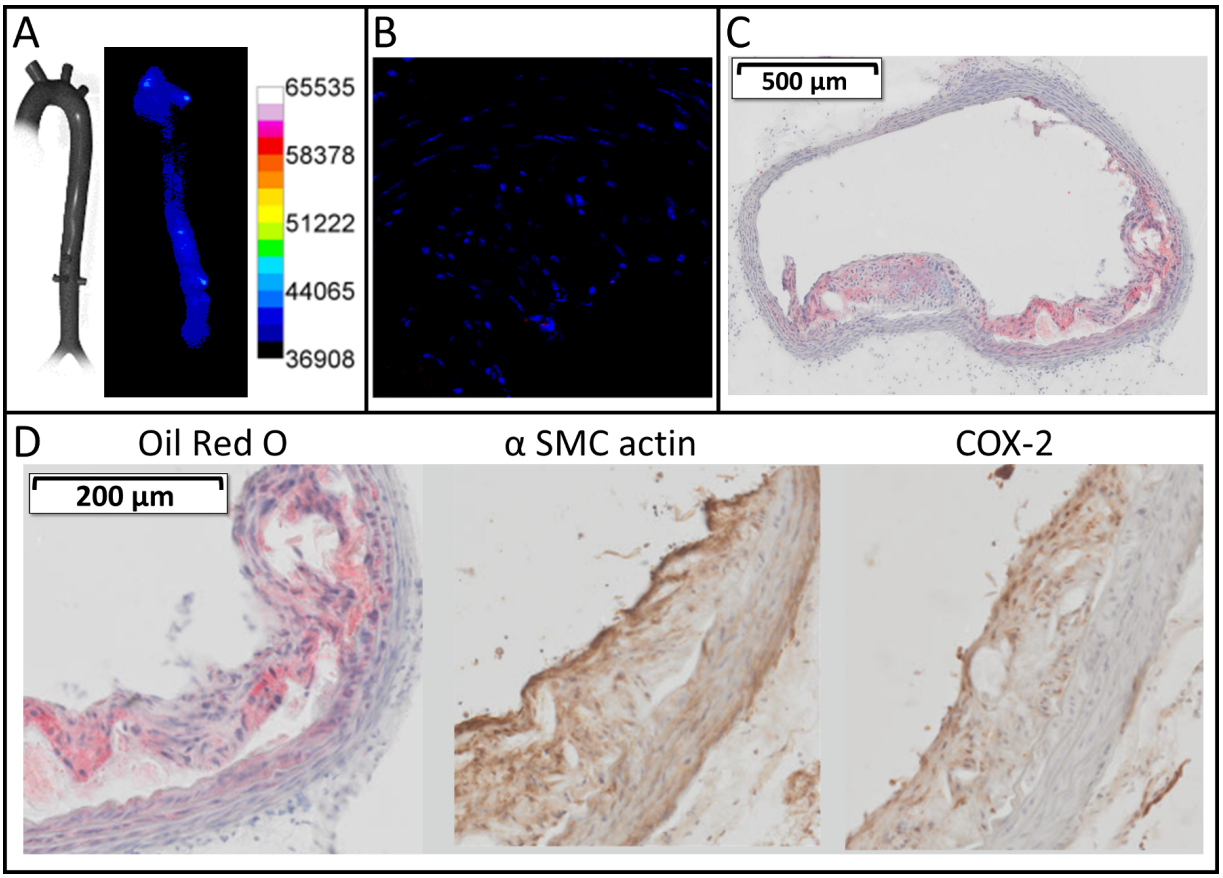

Fig. S9: Aorta localization and histology for ApoE$^{-/-}$ mice treated with control PS_{14}PEG NPs.

NPs based on the control composition PS_{14}PEG were not effective at localizing to areas of atherosclerotic plaques (**A**) and were not seen in plaque cross sections (**B**). PS_{14}PEG NPs were also not effective at reducing aorta occlusion (**C**), or reducing lipid buildup (Oil Red O), neo-intimal hyperplasia (α SMC actin) or inflammation (COX-2) *in vivo* (**D**). Histology of these sections displays similar morphology to non-treated ApoE$^{-/-}$ mice.

Gene	Forward Primer	Reverse Primer
Human ACTB	CAC AGA GCC TCG CCT TTG CCG ATC	ACG AGC GCG GCG ATA TCA TCA TC
Human GAPDH	ATG GGG AAG GTG AAG GTC G	GGG GTC ATT GAT GGC AAC AAT A
Human MSR1	GCA GTG GGA TCA CTT TCA CAA	AGC TGT CAT TGA GCG AGC ATC
Human CD36	GCC AAG GAA AAT GTA ACC CAG G	GCC TCT GTT CCA ACT GAT AGT GA

Fig. S10: Primer sequences used for qRT-PCR.

DETAILED MATERIALS AND METHODS:

Materials. All chemicals/materials were purchased from Sigma-Aldrich (Milwaukee, WI) or Fisher Scientific (Pittsburgh, PA) and used as received unless otherwise noted. 18 MΩ·cm resistivity deionized (DI) water was obtained using PicoPure 2 UV Plus (Hydro Service and Supplies - Durham, NC). The following items were purchased from the indicated vendors: 1.077g/cm^3 Ficoll-Paque Premium from GE healthcare (Pittsburgh, PA), RPMI 1640 from ATCC (Manassas, VA), macrophage colony stimulating factor (M-CSF) from PeproTech (Rocky Hill, NJ), FBS and AlexaFluor 680 carboxylic acid succinimidyl ester from Life Technologies (Grand Island, NY), unlabeled oxLDL from Biomedical Technologies Inc. (Stoughton, MA), 3,3'-dioctadecyloxacarbocyanine (DiO) labeled oxLDL from Kalen Biomedical (Montgomery Village, MD), and human buffy coats from the Blood Center of New Jersey (East Orange, NJ).

NP fabrication and characterization. Kinetically assembled nanoparticles (NPs) were fabricated via flash nanoprecipitation (4-6). Briefly, the amphiphile and the core hydrophobe were dissolved in tetrahydrafuran (THF) before being rapidly mixed with an aqueous stream in a confined impinging jet mixer. The hydrophobe rapidly nucleates, but is stabilized at a monodisperse size by the amphiphiles forming a corona. Unlike micelles, which exisit in thermodynamic equilibrium, the amphiphiles are "locked" around the core by strong hydrophobic interactions. NPs were then dialyzed into PBS for 24 h to remove residual THF and sterile filtered with a 0.45µm nylon filter. NPs were fluorescently labeled by conjugating AlexaFluor 680 (AF680) carboxylic acid succinimidyl ester with amine terminated AMs (6). Selection of amphiphiles to be used in the shell of NPs was based on our previous computational work to predictively design anti-atherogenic biomaterials (2). AMs were chosen based on exhibiting different 3D conformations and diverse molecular features.

Cell culture. Human monocyte derived macrophages (hMDMs) were generated from human peripheral blood mononuclear cells (PBMCs) as described previously (2). Mononuclear cells were isolated from PBMCs by Ficoll-Paque density gradient (1.077g/mL), washed and plated into tissue culture flasks with RPMI 1640 media with 10% FBS and 1% penicillin/streptomycin. Non-adherent cells were washed away after 24 h and remaining monocytes were differentiated into macrophages using 50ng/mL M-CSF for 7 days. Macrophages were then trypsinized, transferred to tissue culture plates at 50,000 cell/cm^2 and allowed to adhere for 24 h before experimental treatment.

***In vitro* inhibition of oxLDL uptake.** NPs were evaluated for efficacy by measurement of oxLDL uptake inhibition in hMDMs following exposure to fluorescent DiO oxLDL (1 µg/mL, Kalen Biomedical) and unlabeled oxLDL (4 µg/mL, Biomedical Technologies) with or without NPs (10^{-5} M) for 24 hours in base media. Cells were collected by vigourous pipetting with cold 2mM EDTA in PBS, centrifuged and fixed in 1% PFA. OxLDL uptake was determined using a Gallios flow cytometer (Beckman Coulter) and analyzed with FlowJo software (Treestar), quantifying the DiO MFI of intact single cells. A minimum of three experimental replicates was conducted for this study, each from a

different cell donor, with >10,000 cells per replicate. Data was background subtracted and is presented as normalized % oxLDL uptake, determined by the following equation:

$$\%\ oxLDL\ Uptake = 100 * \frac{\text{DiO oxLDL MFI of treatment sample}}{\text{DiO oxLDL MFI of oxLDL only control sample}}.$$

For microscopy, cells were washed with PBS, fixed in 4% PFA, and counterstained with Hoechst 33342 before imaging on a Leica TCS SP2 confocal microscope. Representative images were prepared with ImageJ.

***In vitro* NP binding via scavenger receptors.** NPs were evaluated for binding to macrophage scavenger receptors using hMDMs. hMDMs were incubated with polyinosinic acid (10 μg/mL, Sigma Aldrich), CD36 monoclonal antibody (2 μg/mL, clone JC63.1, Cayman Chemical) or isotype control to human CD36 antibody, purified mouse IgA, κ (BD Pharmigen, clone M18-254) in base media for 1 h at 37 °C. Following the incubation, blocking agents were removed, cells washed, and then incubated with fluorescent NPs (10^{-5} M, with 5% of shell AM labeled with AlexaFlour 680) of distinct compositions for 6 h. Cells were collected by vigourous pipetting with cold 2mM EDTA in PBS, centrifuged and fixed in 1% PFA. NP uptake was determined using a Gallios flow cytometer (Beckman Coulter) and analyzed with FlowJo software (Treestar), quantifying the AF680 MFI of intact single cells. A minimum of three experimental replicates was conducted for this study, each from a different cell donor, with >10,000 cells per replicate. The degree of inhibition of NP uptake caused by each blocking agent was determined by the following equation:

$$\%\ NP\ Uptake = 100 * \frac{\text{NP MFI sample pretreated with blocking agent}}{\text{NP MFI sample not pretreated with blocking agent}}.$$

For microscopy, cells were washed with PBS, fixed in 4% PFA, and counterstained with Hoechst 33342 before imaging on a Leica TCS SP2 confocal microscope. Representative images were prepared with ImageJ.

***In vitro* NP modulation of scavenger receptors.**

NPs were evaluated for modulation of scavenger receptor expression using hMDMs. hMDMs were incubated with unlabeled oxLDL (5 μg/mL) with or without NPs of each chemistry for 24 h. Cells were collected by vigourous pipetting with cold 2mM EDTA in PBS and washed in blocking buffer (0.5% bovine serum albumin (BSA), 0.1% sodium azide, and 1% normal goat serum in PBS). Cells were centrifuged, supernatants were decanted and the cells were incubated for 1 h at 4°C with PE anti-human SR-A1 antibody (clone 351615, R&D Systems) and APC anti-human CD36 antibody (clone: 5-271, Biolegend) or their corresponding isotype controls APC mouse IgG2a, κ (clone: MOPC-173, Biolegend) and PE mouse IgG2B (clone 133303, R&D systems). Following antibody incubation, the cells were washed, centrifuged and fixed in 1% PFA. SR expression was determined using a Gallios flow cytometer (Beckman Coulter) and analyzed with FlowJo software (Treestar), quantifying the PE and APC MFI of intact single cells. A minimum of three experimental replicates was conducted for this study, each from a different cell donor, with >10,000 cells per replicate. The change in scavenger receptor expression was determined by the following equation:

$$\%\ SR\ Expression = 100 * \frac{\text{SR MFI of treatment sample}}{\text{SR MFI of oxLDL only control sample}}.$$

For microscopy, cells were washed with PBS, fixed in 4% PFA, and then blocked with 0.5% bovine serum albumin (BSA), 0.1% sodium azide, and 10% normal goat serum in PBS for 2 h. Next, cells were

incubated for 3 h at room temp with primary antibodies and isotypes used for flow cytometry. Following the incubation they were washed and then incubated with secondary antibodies: goat anti-mouse IgG2α alexa fluor 488 (SR-A1 conditions) or goat anti- mouse IgG2β alexa fluor 647 (CD36 conditions) for 1 h. Cells were then washed, and counterstained with Hoechst 33342 before imaging on a Leica TCS SP2 confocal microscope. Representative images were prepared with ImageJ.

***In vitro* NP modulation of scavenger receptor gene expression.** NPs were evaluated for modulation of scavenger receptor gene expression using hMDMs. hMDMs were incubated with unlabeled oxLDL (5 μg/mL) with or without NPs of each chemistry for 24 h. RNA was extracted using the RNeasy Plus Mini Kit (Qiagen) following the manufacturers protocol. cDNA was synthesized with the High Capacity RT kit (Life Technologies). Primer sequences were obtained from Harvard Primer Bank and synthesized by Integrated DNA Technology. qRT-PCR was performed on a Lightcycler 480 using Fast SYBR Green Master Mix (Life Technologies) for 40 cycles. C_t values were obtained by 2^{nd} derivative maxima and fold change was calculated with ΔΔCt. GAPDH and ACTB were used as endogenous controls and oxLDL only treated cells were used as the basal control condition for normalization.

Correlation analysis and atheroprotective potency ranking. Efficacy data for oxLDL uptake inhibition, NP uptake by MSR1, NP uptake by CD36, downregulation of MSR1 surface expression and downregulation of CD36 surface expression were converted into a database in Molecular Operating Environment (MOE) v. 2013.08 (Chemical Computing Group). A correlation matrix was calculated for all biological descriptors in MOE. For ranking of cumulative atheroprotective potency, all *in vitro* efficacy values were normalized, weighted equally and summed for each NP formulation. NPs were rank ordered and the highest performing NP (M_{12}PEG) was selected for further studies.

Computational model. Quantitative structure activity relationship (QSAR) models were generated as previously described (2). Briefly, detailed 3D structures of AMs were computed previously by a two-step molecular dynamics simulation using a coarse-grain model for 400 ns followed by a detailed all-atom energy minimization for 10 ns. Molecular descriptors were extracted from the 3D structures using Dragon v.5.4 (Talete) and Molecular Operating Environment (MOE) v. 2013.08 (Chemical Computing Group). Descriptors were selected and correlated with variations in biological activity (oxLDL uptake, CD36 and MSR1 gene expression, CD36 and MSR1 cell surface receptor expression, and NP uptake by CD36 and MSR1) using a partial least squares analysis in MOE.

Animals and administration of NPs. 4 week old B6.129P2-*Apoe*^{tm1Unc} (ApoE$^{-/-}$) and C57B/L6 mice purchased from Taconic were given free access to food and water. The Institutional Committees on Animal Care and Use at Rutgers University approved all procedures involving animals (protocol # 06-016). ApoE$^{-/-}$ mice were fed Harlan Teklad diet TD.88137, a Western diet (21% fat, 34% sucrose, and 0.2% cholesterol) (7). C57B/L6 mice were given standard chow diet. For NP administration, mice were anesthetized with isoflurane and given tail vein injections (5 μL/g body weight) of NPs at $7.5*10^{-4}$ M (8). Mice were dosed a total of 4 times in 8 day intervals, beginning at 8 weeks after initiation of the high fat diet (**Fig. 3A**). The dosing regimen was developed to ensure a minimum therapeutic

concentration of 10^{-7} M, assuming a 24 h half-life. ApoE$^{-/-}$ treatment and no treatment groups had n=5, C57B/L6 had n=3.

Animal imaging. To determine biodistribution over time, mice were anesthetized with 2.5% isoflurane by inhalation and imaged using a MultiSpectral FX Pro In Vivo Imager (Carestream) before NP administration and at 1, 2, 4, 8, 10, 18 and 26 days after the initial NP administration. Fluorescence images were taken with the following settings: Ex 650, Em 700, 30 s exposure with 10 s X-Ray exposure to visualize anatomy.

Animal euthanasia. At 8.5 weeks after initiation of treatment, mice were anesthetized with 2.5% isoflurane by inhalation and sacrificed by cardiac puncture and perfusion with phosphate buffered saline (PBS). The aorta, heart, liver, kidneys, lungs, intestines and adipose were excised and immediately imaged using a MultiSpectral FX Pro. The tissues were then preserved in RNALater (for gene expression analysis), preserved in formalin (for immunohistochemistry) or homogenized, strained, and stained (for flow cytometry). The aorta was divided into three sections for analysis; ascending aorta and aortic arch for immunohistochemistry, thoracic aorta for PCR and abdominal aorta for flow cytometry. Blood was allowed to clot for 30 minutes at room temp, and serum was separated by centrifugation

NP cellular association and receptor expression using flow cytometry. Tissues were homogenized (Tissue Tearor) and then passed through a 40 μm cell strainer and washed with PBS. Solids were allowed to settle for 2 min and the cell suspension removed. Cells were blocked with PBS buffer containing 0.5% bovine serum albumin, 0.1% sodium azide, and 1% normal goat serum for 30 min. Following blocking they were incubated with labeled antibodies against CD68, VCAM1 and α-smooth muscle actin (Biolegend) for 1 hour at 4°C. After the incubation they were washed twice with PBS, incubated with CyTRAK Orange (eBioscience) for 30 min, fixed in 200 μL of 1% paraformaldehyde, and then quantified (10,000 cellular events per sample) using a Gallios flow cytometer (Bekman Coulter). Samples were quantified using the geometric mean fluorescence intensity (MFI) of intact cells with FloJo (Treestar).

Aorta tissue preparation for imaging and immunohistochemistry. The ascending aorta and aortic arch were sectioned serially to examine plaque morphology and binding of AM NPs to lesions via microscopy. Aortas from treated mice were fixed in formalin and prepared for cryosectioning by immersion in 30% sucrose. Tissue was embedded in OCT media (Tissue Tek), frozen and sectioned into 10 μm serial sections on a cryostat (Thermo Electron). Slides were imaged with an Olympus VS120. Serial aortic cross sections were quantified for total area and plaque area using VS-AFW software (Olympus). The reduction in plaque burden was calculated with the equation:

$$Reduction\ in\ plaque\ burden = 100 - 100 * \frac{plaque\ area\ of\ NP\ treated\ mice}{plaque\ area\ of\ untreated\ mice}.$$

NP accumulation was evaluated on a Leica TCS SP2 confocal microscope using a 63x oil immersion objective following counterstaining with ProLong Gold with DAPI (Life Technologies).

Aortic cross sections were analyzed for lipid accumulation and markers of neointimal formation and inflammation. To visualize areas of lipid deposits, sections were washed in 60%

isopropyl alcohol before staining with 3 mg/mL Oil Red O in 60% isopropyl alcohol and counterstaining with Mayers hematoxylin. Oil Red O sections were coverslipped with Prolong Gold. To determine neointimal formation and levels of inflammation in tissue, sections were incubated with rabbit polyclonal anti cyclooxygenase 2 (Abcam, ab15191), anti α-smooth muscle actin antibodies (Abcam) or rabbit control IgG (Pro-Sci). Sections were delipidized in xylene (9 min) and a decreasing series of alcohol (2 min each) for before neutralization with 3% H_2O_2, followed by washing and blocking with goat serum (100% for COX-2 and 25% for αSMA) with streptavidin (Vector Labs) for 2 h at room temp. Sections were incubated with primary antibodies (1μg/mL COX-2, 0.4μg/mL SMC α-actin) in blocking buffer with biotin (Vector Labs) overnight at 4°C, and then washed before secondary incubation with Vectastain Elite anti-rabbit IgG (Vector Labs). Staining was visualized with DAB peroxidase (Vector Labs) and counterstained with Mayers Hematoxalin for 3 min. Sections were coverslipped with permount and imaged with an Olympus VS120.

For *en face* imaging of NP localization, the aortic tree was dissected out 24 h after administration of NPs. Tissues were fixed in formalin and adventitia was removed before the aorta was opened *en face* and pinned to a PDMS plate. Fluorescence and reflected light images were captured on a Nikon TE2000S, overlaid in ImageJ and joined using Image Composite Editor (Microsoft).

1. Kunjathoor VV*, et al.* (2002) Scavenger receptors class A-I/II and CD36 are the principal receptors responsible for the uptake of modified low density lipoprotein leading to lipid loading in macrophages. *J. Biol. Chem.* 277(51):49982-49988.
2. Lewis DR*, et al.* (2013) In silico design of anti-atherogenic biomaterials. *Biomaterials* 34(32):7950-7959.
3. Consonni V & Todeschini R (2000) *Handbook of molecular descriptors* (Wiley-VCH, Weinheim ; New York) pp xxi, 667 p.
4. Johnson BK & Prud'homme RK (2003) Flash NanoPrecipitation of Organic Actives and Block Copolymers using a Confined Impinging Jets Mixer. *Aust. J. Chem.* 56(10):1021-1024.
5. Liu Y, Cheng C, Liu Y, Prud'homme RK, & Fox RO (2008) Mixing in a multi-inlet vortex mixer (MIVM) for flash nano-precipitation. *Chem. Eng. Sci.* 63(11):2829-2842.
6. York AW*, et al.* (2012) Kinetically Assembled Nanoparticles of Bioactive Macromolecules Exhibit Enhanced Stability and Cell-Targeted Biological Efficacy. *Adv. Mater.* 24(6):733-739.
7. Whitman SC (2004) A practical approach to using mice in atherosclerosis research. *Clin. Biochem. Rev.* 25(1):81-93.
8. Diehl K-H*, et al.* (2001) A good practice guide to the administration of substances and removal of blood, including routes and volumes. *J. Appl. Toxicol.* 21(1):15-23.